

Optical spectroscopy of $\text{La}_3\text{Ga}_5\text{SiO}_{14}:\text{Cr}^{3+}$ crystals

M. Casalboni,* A. Luci, and U. M. Grassano

Dipartimento di Fisica, Università di Roma "Tor Vergata," Via della Ricerca Scientifica, 1, 00133 Rome, Italy

B. V. Mill and A. A. Kaminskii

Institute of Crystallography, Russian Academy of Sciences, Moscow, Russia

(Received 29 July 1993)

The optical properties of trivalent chromium ions in $\text{La}_3\text{Ga}_5\text{SiO}_{14}$ crystals have been investigated by means of absorption, emission, excitation, and lifetime measurements. The particular intermediate value of the octahedral crystal field $Dq/B \sim 2.5$ causes the overlapping of the 4T_2 with the 2E and 2T_1 levels. This overlap is the origin of Fano resonances in the absorption spectrum and of the simultaneous presence of broadband and narrow-line emissions. Polarized measurements have allowed the determinations of second-order effects such as the tetragonal or orthorhombic distortion of the octahedron of oxygen ions around the chromium ion. Moreover the temperature shift of the peak and the nonexponential decay of the broad emission band are indications of the disorder present in the crystal lattice. All these results produce a fairly complete picture of the energy levels of Cr^{3+} ions in a typical crystal of the Ca-gallogermanate family.

I. INTRODUCTION

In recent years the study of the optical properties of crystals and glasses, containing trivalent chromium, has received a new impulse connected both to the exploitation of these materials as active media for infrared tunable laser, and to the fundamental understanding of the interaction between impurity and host lattice.¹⁻⁷

In the crystalline systems the experimental data can be interpreted by means of the *crystal field theory*. The energy positions of the Cr^{3+} absorption bands and in particular the emission properties, the most interesting feature for laser physics, are strongly dependent upon the value of the crystal field. Its intensity determines which is the lowest, among the various excited states, and therefore which kind of emission (narrow line or broadband) predominates.

If the host crystal or the impurity site symmetry is lower than cubic one can perform polarized absorption and emission measurements. These data yield information regarding, for instance, the electric or magnetic dipole character of the transitions.

The $\text{La}_3\text{Ga}_5\text{SiO}_{14}$ crystal belongs to the Ca-gallogermanate family and has a trigonal D_3^2 symmetry with a and c lattice parameters of 8.162 and 5.087 Å, respectively. The Cr^{3+} impurity replaces the Ga^{3+} ion. His nearest neighbors are six oxygen atoms in an octahedral coordination and therefore the most relevant symmetry of the crystal field around the Cr^{3+} ion is the O_h symmetry. In the first coordination shell there are Ga^{3+} and La^{3+} ions in a regular lattice site. In the second coordination shell instead, Ga^{3+} and Si^{4+} ions are statistically distributed among equivalent sites giving origin to the structural disorder of this family of crystals. A detailed description of the structure of this crystal is reported in Ref. 8. Preliminary spectroscopic measure-

ments and lasing performances on this system were already published.^{7,9}

In this paper we present a new and more detailed study on the optical properties of Cr^{3+} ion in the $\text{La}_3\text{Ga}_5\text{SiO}_{14}$ crystal. In particular we have performed absorption, emission, excitation and lifetime measurements from which we derive a complete description of the Cr^{3+} energy levels.

II. ENERGY TRANSITIONS OF Cr^{3+} IN QUASIOCTAHEDRAL SITES

The Cr^{3+} ion has, in the outermost orbit, an electronic configuration d^3 , yielding a ground state 4F and, at higher energy, other quartet and doublet states: the next terms in order of increasing energy are 4P and 2G .

When the Cr^{3+} ion is placed in an insulating (ionic) crystal as an impurity activator, it commonly occupies an octahedral site. The position of the Cr^{3+} energy levels is determined by two factors: the electrostatic interaction between the equivalent d electrons and the crystal field interactions, mainly due to the nearest-neighbor ions of the lattice (the *ligand* ions). In the complete Hamiltonian describing the ion, these two terms are comparable in magnitude and therefore the system can be treated only in an intermediate field approximation.^{10,11}

In a cubic field the sevenfold orbitally degenerate 4F state is split into the 4A_2 , 4T_2 , and 4T_1 levels. The energy difference between the 4A_2 ground state and 4T_2 is by definition called $10Dq$ and its value is a measure of strength of the crystal field. Also the energy of 4T_1 strongly varies with the crystal field. The low-spin states are also split by the crystal field and for example the 2G state is divided into 2E , 2T_1 , 2T_2 , and 2A_1 states. Their dependence on the field intensity is less marked and the

2E and 2T_1 energy distance from the ground state is almost constant at all fields.

Sometime the energy states are named following a different (one-electron) picture: every fivefold degenerate d electron orbital is split by the octahedral field into a lower triply degenerate t_{2g} state and a higher doubly degenerate e_g state. The lowest configuration (ground state) is formed by three electrons (with parallel spin) in the t_{2g} orbital. The next higher configurations are formed by the orbital combinations $t_{2g}^2e_g$, $t_{2g}e_g^2$, and they may contain quartet or doublet terms. The latter description is correct if the crystal field is so strong that one can neglect the Coulomb interaction between the d electrons (strong field limit).

In the other cases one must diagonalize the Hamiltonian taking into account both interactions simultaneously as done by Tanabe and Sugano¹² who gave a complete calculation for all the d -electron configurations in the cubic field. The well-known Tanabe-Sugano diagrams that follow from the theory show the energy of the electronic states as a function of the crystal field intensity from zero (free ion) to the strong field limit. Both the energy levels and the crystal field are usually represented in units of B (the B Racah parameter) and the energies of the excited states are plotted with respect to the ground state (the abscissa line). Spin-orbit and phonon coupling are neglected in this model. Transitions can occur between the levels, consistently with the selection rules.

Figure 1 shows the Tanabe-Sugano diagram for the Cr^{3+} ion in $\text{La}_3\text{Ga}_5\text{SiO}_{14}$. The energy levels of the d^3 configuration are calculated from the Dq , B , and C values obtained by means of the spectroscopic data of the present paper (see below). Only the lowest levels are shown.

If the impurity site is not perfectly octahedral, as commonly occurs in many host crystals, the local distortions cause a further reduction of the symmetry, producing in turn a splitting of the degenerate levels. To this interesting aspect is devoted the fundamental article of Yamaga

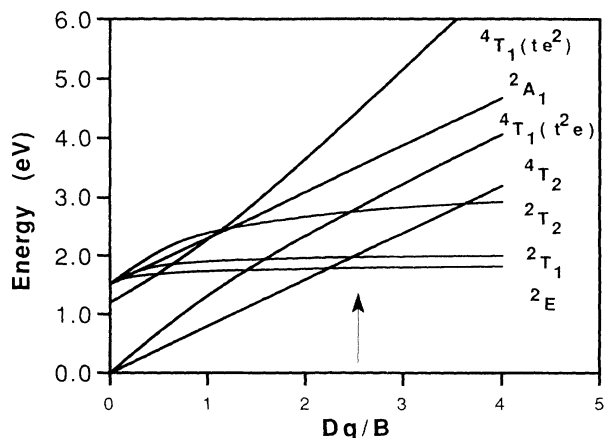


FIG. 1. Energy levels of a d^3 ion in octahedral crystal field. The diagram has been plotted using the value $\frac{C}{B} = 5.1$. The arrow indicates the value of $\frac{Dq}{B} = 2.5$ calculated for the $\text{La}_3\text{Ga}_5\text{SiO}_{14}$ crystal.

*et al.*⁶ where a molecular orbital theory is developed to understand how these distortions produce the observed polarization properties.

The emission properties of d^n ions, and in particular of Cr^{3+} doped crystals, were extensively studied in view of their use in the development of laser sources. The emission band shape is strongly dependent on the value of the crystal field: for weak fields, the relaxed excited state, from which the emission of the Cr^{3+} ion takes place, is the 4T_2 state that possesses a relatively short lifetime ($\sim 1 \mu\text{s}$) and produces broad infrared emission bands. For stronger fields, the lowest relaxed excited state is the 2E level (see Fig. 1), that is almost insensitive to the crystal field value and to the vibrations, producing a much narrower band (the so-called *R line*). Moreover the emission lifetime results of the order of milliseconds because the transition is spin forbidden.

In some cases, as in the present one of $\text{La}_3\text{Ga}_5\text{SiO}_{14}:\text{Cr}^{3+}$, both emissions are simultaneously present: beside a broad IR band, a much narrower emission band at high energy is visible, although with a very low intensity.

Such an occurrence allows one to investigate, from the dependence of the emission band intensities upon the sample temperature, other important properties of the Cr^{3+} energy levels such as the shape of their *adiabatic potential energy surfaces*.

III. EXPERIMENTAL RESULTS

A. Absorption measurements

Single crystals of $\text{La}_3\text{Ga}_5\text{SiO}_{14}:\text{Cr}^{3+}$ were grown by the Czochralski method from the melt using platinum crucible. In the investigated samples the Cr^{3+} concentration was about 1%. The absorption spectra were obtained by means of a Perkin Elmer Lambda 19 spectrophotometer, modified in order to perform polarized measurements, in the temperature range 10–300 K.

Three series of absorption measurements at various temperatures were performed. The experimental conditions differ with respect to the relative orientation between the polarization state of the light and the direction of the sample c axis: electric field parallel to the c axis (π spectrum); magnetic field parallel to the c axis (σ spectrum); electric and magnetic field both perpendicular to the c axis (α spectrum). In all these experimental configurations two main absorption bands are observed and attributed (see Fig. 2) to the ${}^4A_2 \rightarrow {}^4T_2$ and ${}^4A_2 \rightarrow {}^4T_1$ transitions with peak position at approximately 2.0 and 2.8 eV, respectively. The absorption above 4 eV includes a further Cr^{3+} ion transition (see below), but consists mainly of band to band absorption of the host crystal.

The temperature dependence of all the spectra is rather small resulting in a 25% reduction of the intensity between 15 and 300 K. In contrast to this smooth decreasing trend, the 2.00 eV absorption band in the π spectrum increases from 10 to ~ 120 K and decreases with further warming of the sample up to room temperature.

The α and σ spectra are almost coincident while the π spectrum differs in band positions and relative heights. In particular the low-energy band of the π spectrum has an intensity four times larger than in the other polarizations. The high-energy component, instead, though of comparable intensity, is remarkably broader, in the π spectrum, and his peak appears shifted in energy with respect to the corresponding band obtained in the other spectra.

In order to reach a more quantitative understanding, a fitting of the experimental curves with theoretical band shapes was undertaken.

Figure 3 shows the deconvolutions of the 15 K absorption spectra for the three polarizations. We used the Pekar-band shape¹³ and not the more symmetrical Gaussian shape, typical of the color centers, because of the intermediate value of the electron-lattice coupling in the present case. The Pekar-band shape is defined by

$$\alpha_S(\omega) = \frac{\alpha_0 e^{-S} S^p}{p!}, \quad (1)$$

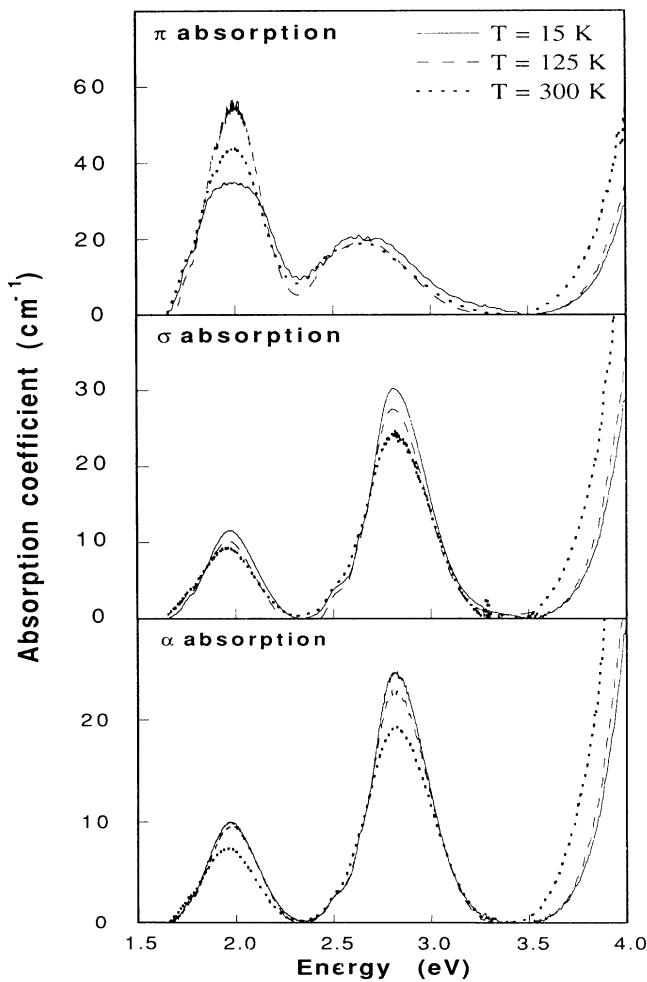


FIG. 2. Absorption spectra of the $\text{La}_3\text{Ga}_5\text{SiO}_{14}:\text{Cr}^{3+}$ crystal for different polarization directions of the measuring light with respect to the crystal c axis (see text). Measurements were performed at 15 K (full line), 125 K (dashed line), and 300 K (dotted line).

that, using the Stirling approximation for the factorial, can be reduced to

$$\alpha_S(\omega) = \frac{\alpha_0 e^{-(S+p)} S^p}{p^p \sqrt{2\pi p}}. \quad (2)$$

The continuous variable p represents an effective vibrational level of the electronic excited state reached in the transition and is related to a zero-phonon transition at $\hbar\omega_0$ and to the average phonon energy $\hbar\bar{\omega}$ by

$$p = \frac{\omega - \omega_0}{\bar{\omega}}. \quad (3)$$

S is the Huang-Rhys factor representing the average number of phonons emitted in the relaxation towards the *relaxed excited state* (RES); α_0 is related to the intensity of the band.

This procedure clearly shows the difference in the peak energies of the π spectrum with respect than of the α and σ spectra and the presence of a new band between the main ones in all the absorption spectra. This band, with peak position at approximately 2.6 eV, is attributed to

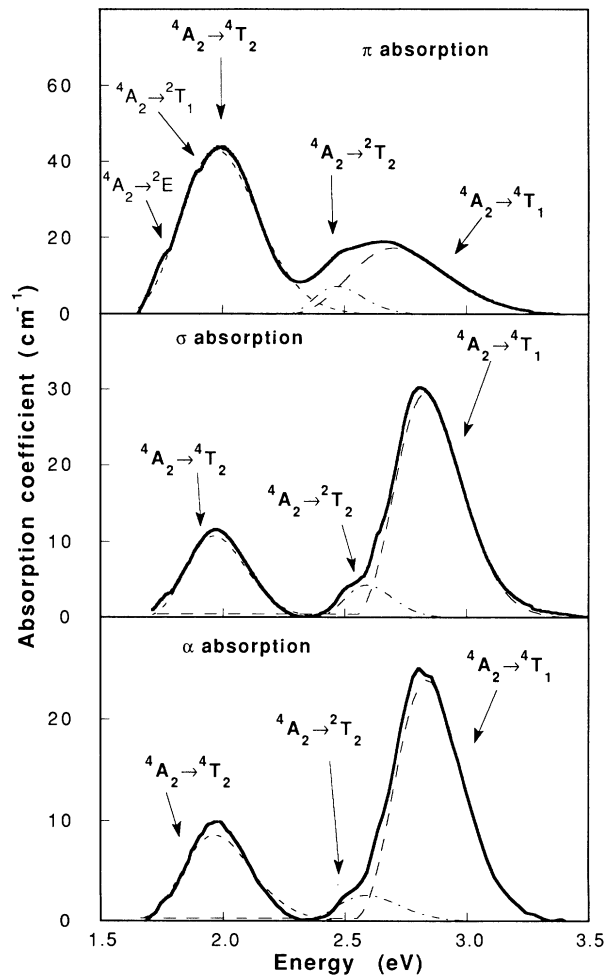


FIG. 3. Absorption spectra at 15 K for different polarizations fitted to a sum of different bands with Pekar line shapes. The assignments to transitions in an octahedral fields are indicated.

the ${}^4A_2 \rightarrow {}^2T_2$ transition (see below). Table I summarizes the values obtained from the fitting.

Other interesting features shown by the absorption spectra are some irregularities in the band shape present mainly in the low-energy band. These irregularities are attributed to the so-called *Fano antiresonances* that arise when a narrow level is degenerate with a broad continuum of states.^{14–16} In our case we assume that the 2E and 2T_1 levels are degenerate with the phonon broadened 4T_2 level.

B. Emission spectra

The luminescence measurements were obtained illuminating the sample with a 1 mW CW, linearly polarized He-Ne laser. These measurements, taken at different temperatures, were corrected for the sensitivity of the detection apparatus. A preliminary report of these emissions has been already presented⁹ and a brief summary is enclosed here for the sake of completeness.

The main emission (Fig. 4) consists of a broadband ranging from 1.1 and 1.6 eV. This luminescence is almost independent from the relative direction of the polarization of the exciting light and the c axis of the crystal. On increasing temperature the intensity of the band decreases and the band shape presents a small broadening and blueshift of the peak energy. On the high-energy side, a second band is present: it is a dim band, peaked at 1.783 eV whose intensity is more strongly dependent upon the temperature. We attributed these two bands to the ${}^4T_2 \rightarrow {}^4A_2$ and ${}^2E \rightarrow {}^4A_2$ transitions, respectively, the latter being allowed by level mixing.^{17–20}

In Fig. 4 the low-energy absorption band is plotted together with the emission bands. The energy position of the narrow emission band exactly corresponds with one of the Fano antiresonance, supporting the interpretation of this structure as due to the ${}^4A_2 \rightarrow {}^2E$ transition.

Measurements performed in order to verify the polarization degree of the emitted light gave, for the broad and more intense ${}^4T_2 \rightarrow {}^4A_2$ band, a partial (20%) polarization of the emission with vector \mathbf{E} parallel to the c axis, irrespective to the polarization direction of the exciting radiation.

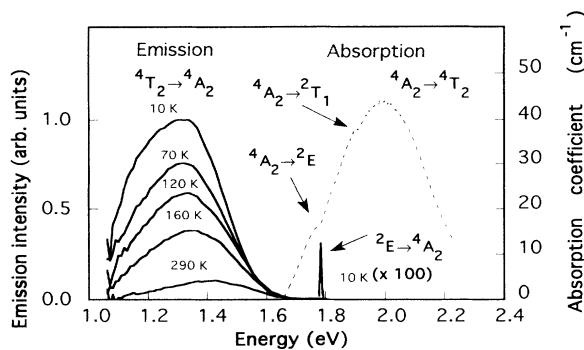


FIG. 4. Emission intensities at various temperatures of the broad and narrow emission bands. The absorption (dotted line) is also shown.

TABLE I. Parameters obtained from the fitting of the experimental absorption bands to Eq. (2). The values obtained for the absorption peaks, $\hbar\omega_{\max}$, are also given.

	Polar.	${}^4A_2 \rightarrow {}^4T_2$	${}^4A_2 \rightarrow {}^2T_2$	${}^4A_2 \rightarrow {}^4T_1$
$\hbar\omega_0$ (eV)	π	1.60	2.29	2.30
	σ	1.67	2.40	2.54
	α	1.68	2.40	2.54
$\hbar\bar{\omega}$ (eV)	π	0.06	0.05	0.09
	σ	0.05	0.05	0.07
	α	0.05	0.03	0.07
S	π	5.7	3.4	4.2
	σ	5.6	4.0	4.2
	α	5.8	4.6	4.2
$\hbar\omega_{\max}$ (eV)	π	1.98	2.47	2.70
	σ	1.96	2.59	2.83
	α	1.96	2.59	2.83
Average		1.97	2.53	2.76

C. Excitation spectra

In order to obtain a deeper knowledge of the whole energy level system of Cr^{3+} in the $\text{La}_3\text{Ga}_5\text{SiO}_{14}$ crystal, we perform a number of excitation spectra of the main luminescence band using a monochromatized 75 W Xenon lamp as an exciting source. The emitted light in the energy range 1.1–1.5 eV was collected filtering the emission with an RG830 Schott filter. The spectra so obtained were corrected in order to normalize the excitation intensity to a constant value. The information so achieved answers three questions: (i) Are there other transitions between the ground state and higher-energy levels? (ii) Is the emission efficiency η constant with the temperature and, if not (iii) how much is the activation energy for the related nonradiative transitions?

The excitation spectra at 15 K taken for the three polarizations are plotted in Fig. 5. Around 4.5 eV a new band is clearly detected. This structure is hardly visible in the absorption spectra, being completely masked by the very high band to band absorption of the crystal

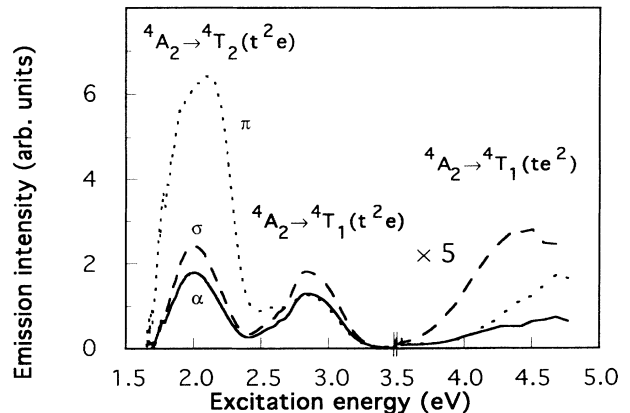


FIG. 5. Excitation spectra at 15 K of the 1.35 eV emission band for various polarizations of the exciting light.

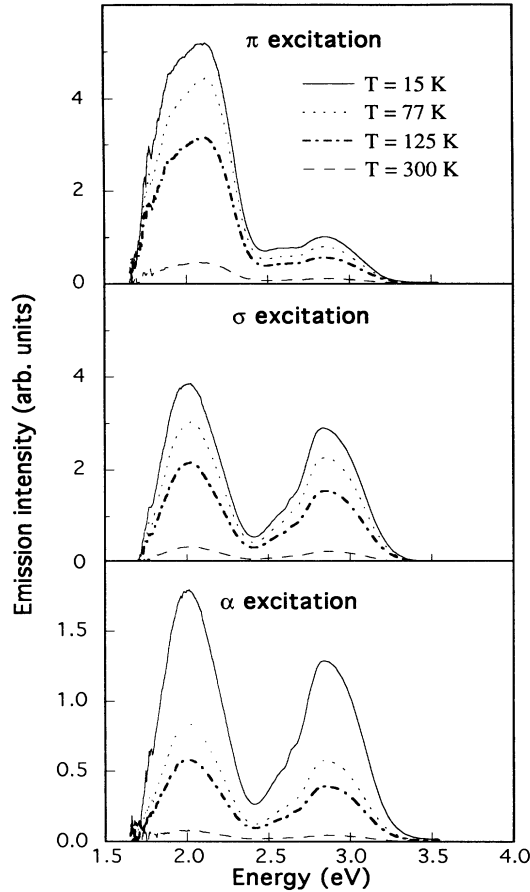


FIG. 6. Excitation spectra of the 1.35 eV emission band for different polarization of the exciting light and different temperatures.

host. The band so observed in the excitation spectrum can be attributed to the ${}^4A_2 \rightarrow {}^4T_1(te^2)$ transition.

Figure 6 shows the excitation spectra of the main luminescence, for the three polarization geometries, as a function of the sample temperature. The behavior clearly evidences that nonradiative processes play an important

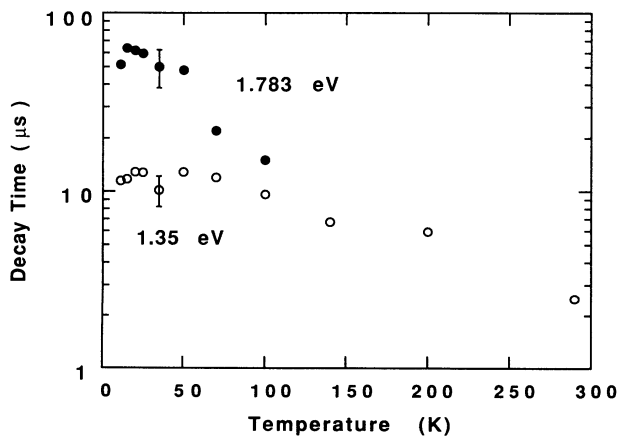


FIG. 7. Decay time of the slow components of the narrow (1.783 eV) and broad (1.35 eV) emission bands as a function of temperature.

role in the deexcitation of the Cr^{3+} ion and they will be treated in detail in the following discussion.

D. Lifetime measurements

The time dependent luminescence intensity was measured after excitation of the sample with a light pulse of 10 ns duration (Lambda Physik Excimer Laser EMG103 with dye laser FL2001 operating with Coumarine 503 at $\lambda = 540$ or 550 nm). In this way one can study the decay time curves for both the broad and the narrow emissions. The curves appear multiexponential, but a fitting with a two-exponential function can allow an evaluation of the complex deexcitation processes. Figure 7 shows, as a function of temperature, the value of the longer component of the lifetime for both emissions. At low temperature the decay time of the 1.783 eV emission is an order of magnitude longer than that of the broad 1.35 eV band.

IV. DISCUSSION

A. Evaluation of crystal field parameters

From absorption and excitation measurements, using the Tanabe-Sugano model a complete level scheme for Cr^{3+} in the $\text{La}_3\text{Ga}_5\text{SiO}_{14}$ crystal host was obtained. A direct indication on the value of the local field Dq can be derived from the average peak energy of the ${}^4A_2 \rightarrow {}^4T_2$ transition (average value of the σ and π absorption spectra):

$$Dq = \frac{E_a({}^4T_2) - E_a({}^4A_2)}{10} = 197 \pm 1 \text{ meV}. \quad (4)$$

Moreover from the average peak energies of the ${}^4A_2 \rightarrow {}^4T_2$ and ${}^4A_2 \rightarrow {}^4T_1$ transitions, the Racah parameter B can be evaluated.^{12,21} Indeed B and Dq are related through the relation

$$\frac{Dq}{B} = \frac{15(x-8)}{x^2-10x}, \quad (5)$$

where the parameter x is defined by the following equation:

$$x = \frac{E_a({}^4T_1) - E_a({}^4T_2)}{Dq}. \quad (6)$$

From the experimental results one obtains

$$x = 4.0 \pm 0.2, \quad (7)$$

$$B = 79 \pm 5 \text{ meV}. \quad (8)$$

The intermediate value of the parameter $\frac{Dq}{B} = 2.5 \pm 0.1$ is consistent with the simultaneous presence of the broad and the narrow emission bands observed in this system.

An estimate of the C Racah parameter can be obtained using the energy value of the absorption transition from the ground state towards the 2E state. The energy of the 2E state indeed depends both upon the parameters

TABLE II. Absorption transition (in eV) measured and evaluated from the Tanabe-Sugano diagram of Fig. 1, based on the position of the 2E , 4T_2 , and 4T_1 energy levels. The first column contains the assignments of the transitions.

Transition	Experimental (eV)	Calculated (eV)
${}^4A_2 \rightarrow {}^2E$	1.79	1.79
${}^4A_2 \rightarrow {}^2T_1$	1.92	1.85
${}^4A_2 \rightarrow {}^4T_2$	1.97	1.97
${}^4A_2 \rightarrow {}^2T_2$	2.55	2.68
${}^4A_2 \rightarrow {}^4T_1(t^2e)$	2.76	2.76
${}^4A_2 \rightarrow {}^4T_1(te^2)$	4.5	4.3

C and B and upon the crystal field value. By means of considerations analogous to those used to value the parameter B we obtain for C the value of 400 ± 20 meV. The ratio $\frac{C}{B}$ results equal to 5.1. The Tanabe-Sugano diagram of Fig. 1 shows the dimensional values (eV) of the ordinate scale because it has been drawn with the above values for the B and C constants.

In Table II we report the calculated and the experimental values for *all* the transitions with the proper attributions. The good agreement between experimental and calculated energy values for 2T_1 , 2T_2 , and ${}^4T_1(te^2)$, that are not used for evaluation of the Tanabe-Sugano diagram, confirms the internal coherence of our assumptions.

B. Lattice distortions

The comparison between the α , π , and σ spectra allows us to attribute an electric or magnetic dipole character to the transitions. When the α and σ spectra are very similar and the π one differs, we are in the presence of *electric* dipole transitions while if the α and π spectra are similar and the σ one differs we are in the case of *magnetic* dipole transition (see for instance p. 437, Ref. 11). In our case we observe a great similarity of the α and σ spectra for all the absorption transitions and hence we assign an electric dipole character to the ${}^4A_2 \rightarrow {}^4T_2$ and ${}^4A_2 \rightarrow {}^4T_1$ transitions. Such an assignment implies that parity and symmetry selection rules are only partially obeyed: static or dynamic distortion of the Cr^{3+} site and level mixing produce the possibility to observe both transitions.

On the other hand, from deconvolutions of the low-temperature absorption spectra (see Fig. 3 and Table I), the small but measurable difference in the values of the energy peak for the σ and π spectra reveals the presence of distortions with respect to a perfect octahedral field that reduces the degeneracy of the levels.

The big difference in the lattice parameters a and c , respectively, 8.162 and 5.087 Å,⁸ suggests as very likely a tetragonal or quasitetragonal distortion. Yamaga *et al.*⁶ have shown that in this case the threefold degenerate 4T_2 (and for analogy 2T_2) levels are split into an orbital singlet 4B_2 and in an orbital doublet 4E level. Likewise the 4T_1 level is split into an orbital singlet 4A_2 and an orbital doublet 4E . The energies of the doublets are higher than those of the singlets in the case of a compression of the

octahedron along its axis, while the order of the levels is reversed in the case of tension along the same axis. Moreover the polarization selection rules indicate a predominant π character of the transitions toward the doubly degenerate states. From Table I we can observe that the doublets (π spectra) are lower in energy than the singlets (σ spectra) in the 4T_1 and 2T_2 transitions by about 0.1 eV. The splitting of the 4T_2 level is not clearly identified from the peak positions, but can be inferred from the values of the $\hbar\omega_0$ energies. We can suppose this is an indication of an elongation along the axis of the oxygen cage surrounding the Cr^{3+} ion. The same kind of measurements are reported for Cr^{3+} ion in YAlO_3 ,⁶ in this case however the π absorption spectra is shifted toward higher energies with respect to the σ spectra. At variance to the present case, moreover, the highest-energy band presents the largest difference between the intensities of the π and σ spectra. The behavior of the ratio of the π and σ spectra is not consistent with a pure tetragonal distortion and has been interpreted as a manifestation of orthorhombic distortions.⁶

The question about the static or dynamic type of distortion can be answered observing the temperature dependence of the absorption spectra. From the small (25%) reduction of the absorption as the temperature rises from 10 to 300 K we can argue that prevalent contribution to the splitting is derived from static distortions.

From the deconvolution of Fig. 3 one obtains a further element useful to the determination of energy levels: the presence of a third absorption band between those peaked at 2.0 and 2.8 eV. We attribute this absorption band to the spin-forbidden ${}^4A_2 \rightarrow {}^2T_2$ transition. Such an attribution follows from the inspection of its energy position in the Tanabe-Sugano diagram, although the half-width is rather broader than expected. Its intensity is low compared to the other transitions in agreement with its spin-forbidden nature.

C. Fano structures and energy levels

Let us now briefly comment on the small structures visible on the low-energy side of the first absorption band (see Fig. 4). We suppose that they are due to the Fano antiresonance structures that modulate the otherwise smooth line shape of the low-energy absorption band. Analogous structures were observed for instance by Sturge *et al.*¹⁵ in V^{2+} doped insulating crystals of KMgF_3 and MgF_2 .

Figure 8(a) shows, on a larger scale, the portion of the absorption spectrum (polarization π) in the 1.65 – 1.95 eV range, where these structures were observed. Figures 8(b) and 8(c) show the experimental points (after subtraction of the fitted Pekarian shape) and their further fitting (full line) following the theoretical analysis of Ref. 15.

The results are a fairly good agreement with the equation

$$\alpha(\omega) - \alpha_B(\omega) = \alpha_0(q^2 + 2\epsilon q - 1)/(1 + \epsilon^2), \quad (9)$$

where we define $\epsilon = (\omega - \omega_r)/\gamma$ with $\hbar\omega_r$ the energy of the discrete level perturbed by the interaction with the continuum and γ^{-1} can be interpreted as a lifetime of the narrow level. The parameter q is connected to the ratio of the narrow and broad transition matrix elements.

Table III summarizes the results of the fitting opera-

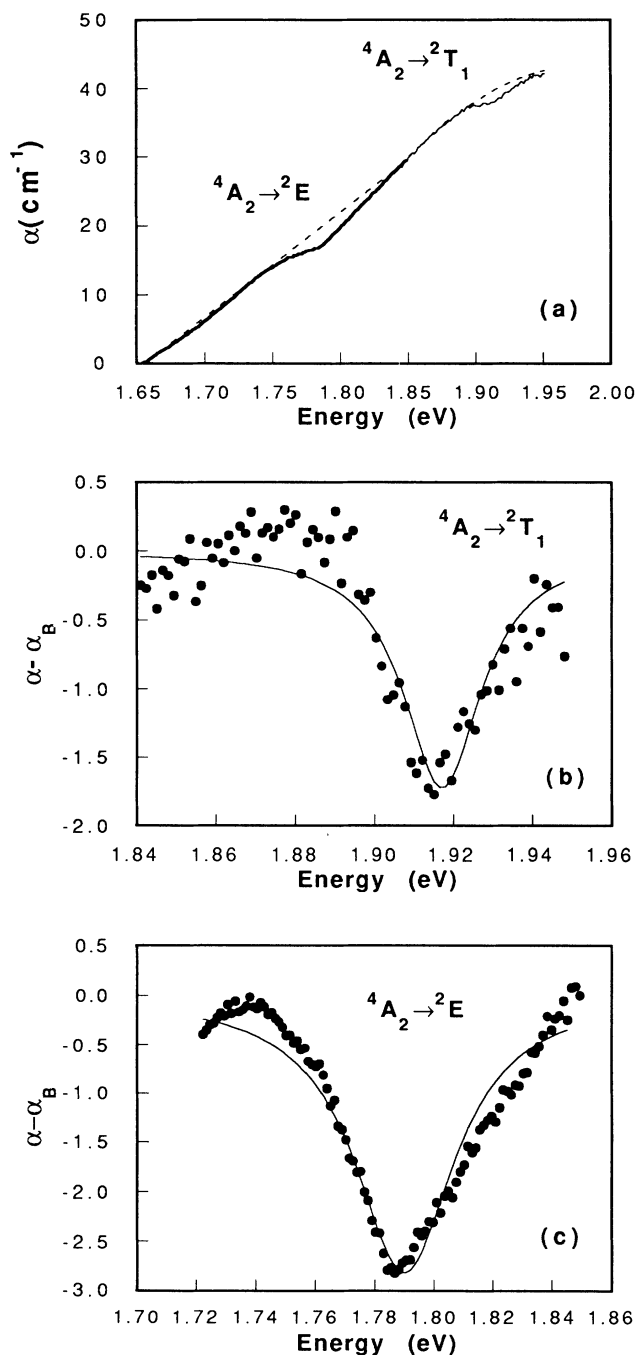


FIG. 8. (a) Absorption spectra (full line) showing, on a broad scale, part of the fitted Pekar line shape (dashed line) (see text). (b) and (c) Difference between the measured and the Pekar line shape of (a). The full line is a fitting with the line shape of the Fano resonances [Eq. (8)] with the parameters reported in Table III.

TABLE III. Fitting parameters of the experimental data (difference between the measured π absorption spectrum and the Pekar line shape) with theoretical expression of Fano resonance [Eq. (8)].

	${}^4A_2 \rightarrow {}^2E$	${}^4A_2 \rightarrow {}^2T_1$
ω_r (eV)	1.79	1.92
$\hbar\gamma$ (eV)	0.02	0.02
q	0.00	0.00
$\frac{\alpha_0}{\alpha_B(\omega_r)}$	0.097	0.045

tion, showing the q parameter next to 0 as expected for a spin-forbidden overlapping a spin-allowed transition, and a fairly large value for γ , comparable to the value obtained in glasses,¹⁶ suggesting some form of structural disorder for the Cr^{3+} sites.

We attribute the structures to the transitions ${}^4A_2 \rightarrow {}^2E$ and ${}^4A_2 \rightarrow {}^2T_1$, as suggested by the emission measurements (see below). Analogous data obtained for a whole set of polarized absorption measurements were performed showing α and σ spectra almost coincident, inside the error introduced mainly by the subtraction of the Pekar background. This indicates an electric dipole character for the transitions toward 2E and 2T_1 levels. It is worth remarking that we cannot observe resonance between the 2T_2 and the 4T_1 levels given that the transition ${}^4A_2 \rightarrow {}^2T_2$ is too broad to produce a Fano resonance.

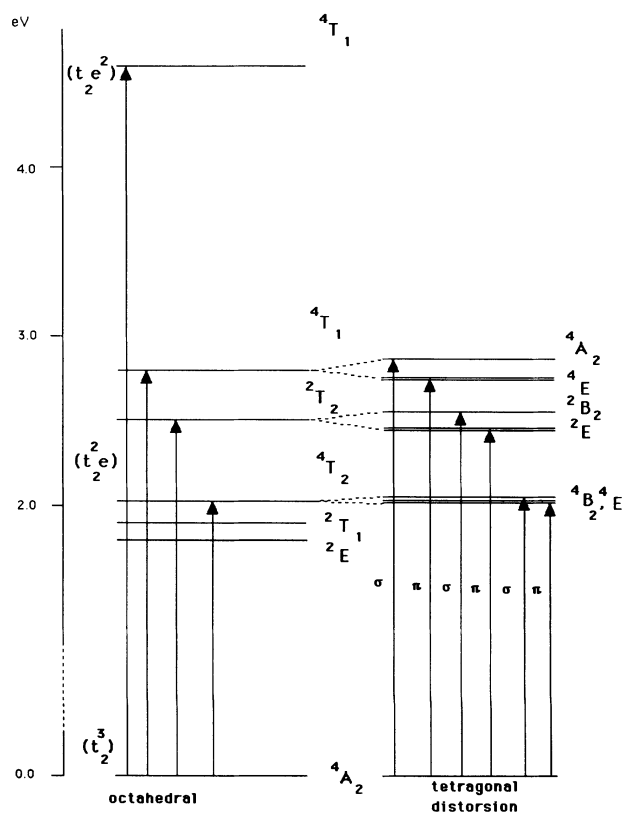


FIG. 9. Energy level diagram of the Cr^{3+} ion in the $\text{La}_3\text{Ga}_5\text{SiO}_{14}$ crystal in the octahedral field approximation (left) and with tetragonal distortion (right).

From the excitation spectra it was possible to extend the range of the level scheme to higher energy, getting information also near the band to band region where the absorption measurements fail to give satisfactory results. From the spectrum of Fig. 5 we observe a new band near 4.5 eV that can be attributed to the ${}^4A_2 \rightarrow {}^4T_1(te^2)$ transition.

The possibility to attribute the electric or magnetic character to this transition is strongly reduced because the information achieved with excitation spectroscopy is indirect: the luminescence efficiency is low and the nonradiative transitions between excited levels become significant and mask information regarding the excitation transitions. This is especially evident in the ${}^4A_2 \rightarrow {}^4T_1(te^2)$ transition at 2.8 eV where the electric dipole character, derived from absorption measurement, is not visible in the excitation spectrum.

The entire energy level scheme of the $\text{La}_3\text{Ga}_5\text{SiO}_{14}:\text{Cr}^{3+}$ crystal resulting from the above considerations is reported in Fig. 9.

D. Emission measurements

The emission of the sample consists mainly in a broad-band in the near infrared region of the electromagnetic spectrum originated by transition from the 4T_2 excited state to the 4A_2 ground state. Such a transition is parity forbidden. Only *odd* vibrations or *odd* static distortions allow the transition to be radiative. The intensity of the emission can be derived from the excitation spectra at different temperatures shown in Fig. 6. It is evident the stronger temperature dependence of the intensity of the excitation spectra with respect to that of the absorption measurements (Fig. 2). This can be related to nonradiative channels that become important as the temperature increases. In Fig. 10 are reported the peak intensities of the π , σ , and α excitations as a function of the inverse of the sample temperature. The experimental data agree with the theoretical curve (full line in the figure)

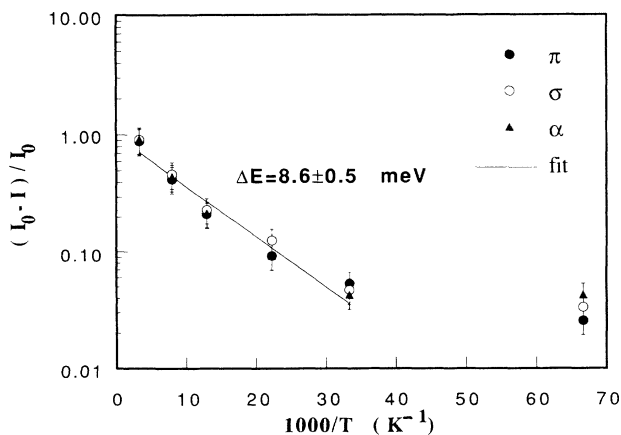


FIG. 10. Arrhenius plot of emission intensity of the 1.35 eV as a function of the reciprocal temperature [see Eq. (9)]. The temperature dependent part shows an activation energy $\Delta E = 8.6$ meV.

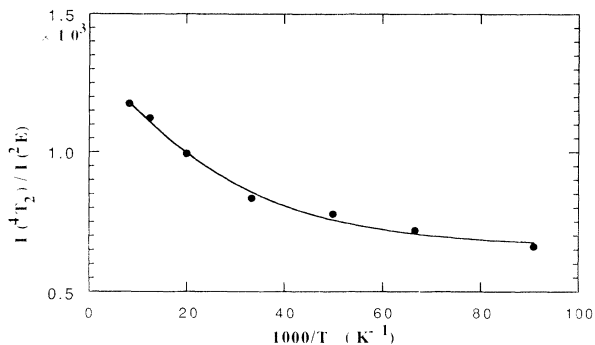


FIG. 11. Ratio of the integrated emission of the broad and the narrow bands, I_T/I_E , as a function of the reciprocal temperature.

$$I = I_0[1 - \exp(-\Delta E/kT)]. \quad (10)$$

Here ΔE is the activation energy of the nonradiative processes and kT is the thermal energy. For all the sets of data we obtain $\Delta E = 8.6 \pm 0.5$ meV. This indicates that a unique mechanism is involved.

Further measurements about the polarization state of the luminescence show that this emission is always partially polarized with an electric vector along the c axis of the crystal, irrespective to the polarization direction of the exciting light and to the absorption transitions excited. This confirms that the emission after relaxation arises mainly from the lowest level.

A very interesting aspect of the luminescence proper-

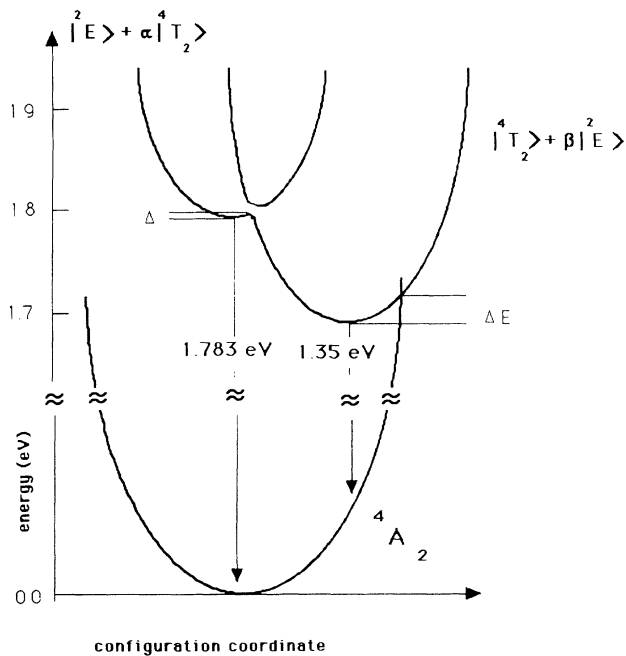


FIG. 12. Potential energy curves for the 4A_2 , 4T_2 , and 2E states in harmonic approximation with linear mixing of the excited states. The activation energies for the quenching of the narrow band, Δ , and of the broadband emission, ΔE , are not drawn to scale.

ties of this system is the occurrence of the narrow emission, at 1.783 eV. This emission has a very low intensity and a stronger temperature dependence with respect to the broad emission band. We attribute this structure to the ${}^2E \rightarrow {}^4A_2$ transition.⁹ This transition should be forbidden (by the spin selection rule); however it can be observed due to a mixing between the 4T_2 and 2E levels produced by the spin-orbit term in the Hamiltonian operator.¹⁸

The plot of the ratio of the integrated intensities of the two emission bands as a function of the temperature is shown in Fig. 11. The procedure illustrated in Ref. 18 permits one to estimate the height of the energy barrier between the 4T_2 and 2E emitting levels and the mixing coefficient. The energy barrier Δ results to be 4.5 ± 0.2 meV and with a mixing coefficient of about 10%.

Figure 12 shows a configuration coordinate diagram in the harmonic approximation for the lower excited states showing the energy barrier Δ between the two emitting states and the activation energy ΔE for the nonradiative transitions.

E. Lifetime measurements

Measurements of the decay of the luminescence excited with a pulsed laser give, as mentioned, nonexponential decay curves. These curves relative to the emission from the 4T_2 and 2E states were recorded and tentatively fitted with a double-exponential function. The slow decay time of the narrow 1.783 emission is, at low temperature, almost an order of magnitude longer than that of the broad 1.35 eV band (see Fig. 7). This difference seems however too small, if compared with the difference in lifetimes between a spin-allowed and a spin-forbidden transition as can be observed in crystals with low and high crystal field. Therefore, in agreement with the simple model described above, we can suppose that the emitting states are derived from a mixing of levels with 4T_2 and 2E symmetry. Other experimental evidences such as the high value of the half-width of the 1.783 eV band and the blueshift with increasing temperature of the broadband emission (see Fig. 4) suggest a more complex description

of this system with some kind of disorder in the chromium neighbors, analogous to that found in silicate glasses.¹⁹ In this case the local field, and therefore the degree of levels mixing, changes from site to site, yielding inhomogeneous broadening of the bands and multiexponential decay behavior for the luminescence.

V. SUMMARY

An extensive study of the optical properties of one of the Ca-gallogermanate-type crystal, $\text{La}_3\text{Ga}_5\text{SiO}_{14}$ containing a Cr^{3+} ion is presented. From absorption, emission, and excitation spectra obtained for different temperatures and in the various polarization directions it was possible to obtain information on the value of the crystal field and on the significant features of the center such as the B and C Racah parameters, the value of the activation energy for the nonradiative transitions toward the ground state, the height of the energy barrier, and the mixing coefficient for the lower excited potential energy curve. Moreover the overlapping of the narrow 2E and 2T_1 levels with the broad 4T_2 band produces two evident structures in the absorption line shape, interpreted as Fano antiresonances.

Most of the data can be interpreted by supposing that the Cr^{3+} ion is surrounded by an octahedron of oxygen ions tetragonally distorted along the c axis. However the complex behavior of the decay of the luminescence, the blueshift with the temperature of the peak energy of the ${}^4T_2 \rightarrow {}^4A_2$ transition, and the widths of the Fano antiresonances suggest a disordered nature of the surroundings of the Cr^{3+} ions.

ACKNOWLEDGMENTS

The authors are indebted to Dr. R. Francini and Dr. A. V. Butashin for the many helpful discussions and advice. They would like also to acknowledge the financial support of this research of the Consiglio Nazionale delle Ricerche (Grant No. 201.11.20 to A.L.) and of the Consorzio Interuniversitario per la Fisica della Materia.

* Permanent Address: Dipartimento di Matematica e Fisica, Università di Camerino, 62032 Camerino (MC), Italy.

¹ B. Henderson and G.F. Imbush, in *Optical Spectroscopy of Inorganic Crystals* (Oxford University Press, Oxford, 1989).

² B. Henderson, A. Marshall, M. Yamaga, K.P. O'Donnell, and B. Cockayne, *J. Phys. C* **21**, 6187 (1988).

³ M. Yamaga, B. Henderson, K.P. O'Donnell, C. Trager Cowan, and A. Marshall, *Appl. Phys. B* **50**, 425 (1990).

⁴ F. Rasheed, K.P. O'Donnell, B. Henderson, and D.B. Hollis, *J. Phys. Condens. Matter* **3**, 2835 (1991).

⁵ R. Balda, J. Fernández, M.A. Illarramendi, M.A. Arriandaga, J.L. Adam, and J. Lucas, *Phys. Rev. B* **44**, 4759 (1991).

⁶ M. Yamaga, B. Henderson, and K.P. O'Donnell, *J. Lumin.*

46, 397 (1990).

⁷ A.A. Kaminskii, A.V. Butashin, A.A. Demidovich, V.G. Koptev, B.V. Mill, and A.P. Shkadarevich, *Phys. Status Solidi A* **112**, 197 (1989).

⁸ A.A. Kaminskii, B.V. Mill, G.G. Khodzhabyan, A.F. Konstantinova, A.I. Okorochkov, and I.M. Silvestrova, *Phys. Status Solidi A* **80**, 387 (1983).

⁹ M. Casalboni, D. de Viry, U.M. Grassano, A.A. Kaminskii, and A. Luci, in *Proceedings of the International Conference on Defects in Insulating Materials*, Nordkirchen, 1992, edited by O. Kanert and J.M. Speth (World Scientific, Singapore, 1993).

¹⁰ A.M. Stoneham, *Theory of Defects in Solids* (Clarendon, Oxford, 1975).

¹¹ D. McClure, in *Solid State Physics*, edited by F. Seitz and

- D. Turnbull (*Academic*, New York, 1959), Vol. 9, pp. 399–525.
- ¹² Y. Tanabe and S. Sugano, *J. Phys. Soc. Jpn.* **9**, 753 (1954); **9**, 766 (1954).
- ¹³ J. J. Markham, *Rev. Mod. Phys.* **31**, 956 (1959).
- ¹⁴ U. Fano, *Phys. Rev.* **124**, 1866 (1961).
- ¹⁵ M.D. Sturge, H.J. Guggenheim, and M.H.L. Pryce, *Phys. Rev. B* **2**, 2459 (1970).
- ¹⁶ A. Lempicki, L. Andrews, S.J. Nettel, B.C. McCollum, and E.I. Solomon, *Phys. Rev. Lett.* **44**, 1234 (1980).
- ¹⁷ C.J. Donnelly, S.M. Healy, T.J. Glynn, G.F. Imbusch, and G.P. Morgan, *J. Lumin.* **42**, 119 (1988).
- ¹⁸ M. Yamaga, B. Henderson, and K.P. O'Donnell, *J. Phys. Condens. Matter* **1**, 9175 (1989).
- ¹⁹ M. Yamaga, B. Henderson, K.P. O'Donnell, and Y. Gao, *Phys. Rev. B* **44**, 4853 (1991).
- ²⁰ M. Yamaga, B. Henderson, and K.P. O'Donnell, *Phys. Rev. B* **46**, 3273 (1992).
- ²¹ B. Sturve and G. Huber, *Appl. Phys. B* **36**, 195 (1985).